

---

# Short and Straight: Geodesics on Differentiable Manifolds

---

**Daniel Kelshaw**  
Imperial College London  
djk21@imperial.ac.uk

**Luca Magri**  
Imperial College London,  
Alan Turing Institute  
l.magri@imperial.ac.uk

## Abstract

Manifolds discovered by machine learning models provide a compact representation of the underlying data. Geodesics on these manifolds define locally length-minimising curves and provide a notion of distance, which are key for reduced-order modelling, statistical inference, and interpolation. In this work, we first analyse existing methods for computing length-minimising geodesics. We find that these are not suitable for obtaining valid paths, and thus, geodesic distances. We remedy these shortcomings by leveraging numerical tools from differential geometry, which provide the means to obtain Hamiltonian-conserving geodesics. Second, we propose a model-based parameterisation for distance fields and geodesic flows on continuous manifolds. Our approach exploits a manifold-aware extension to the Eikonal equation, eliminating the need for approximations or discretisation. Finally, we develop a curvature-based training mechanism, sampling and scaling points in regions of the manifold exhibiting larger values of the Ricci scalar. This sampling and scaling approach ensures that we capture regions of the manifold subject to higher degrees of geodesic deviation. Our proposed methods provide principled means to compute valid geodesics and geodesic distances on manifolds. This work opens opportunities for latent-space interpolation, optimal control, and distance computation on differentiable manifolds.

## 1 Introduction

The manifold hypothesis states that many high-dimensional datasets are expressible on embedded low-dimensional manifolds [1]. Machine learning models which utilise embeddings are well equipped to discover these low-dimensional manifolds and provide compact representation of the underlying data. One notable example of this is the use of autoencoders. It is well-known that an autoencoder with purely linear activations is identical in form to conducting principal component analysis. Introducing nonlinearities increases the expressive power of the network, allowing for a more compact representation [2, 3]. The latent space of the autoencoder provides a set of intrinsic coordinates on the resulting manifold [4].

The composition of transformations defining a model induce a metric which allows for principled operation on the underlying manifold [5, 6]. We can leverage information about the metric to define trajectories on differentiable manifolds that provide some notion of energy-conservation, or length-minimising paths: known as geodesics. Operating on the manifold has numerous consequences, not least: latent-space interpolation for generative modelling [7, 8]; identifying physically-motivated manifolds such as attractors of dynamical systems [9, 10]; measures of similarity and distance [11–13]; as well as the ability to compute statistics on the manifold [14, 15].

In §2 we provide a concise review on differential geometry with a particular focus on Riemannian manifolds and introducing the notion of geodesics. Next, we discuss principled numerical methods

to obtain valid geodesics in §3 and introduce a commonly adopted machine learning method. We apply these methods to find trajectories in the latent space defined by an autoencoder and comment on the validity of the approaches. Finally, we provide a method for computing distance fields, and geodesic flows on differentiable manifolds in §4, based on manifold-informed extensions to the Eikonal equation.

## 2 Review on Differential Geometry

Operating on Euclidean spaces is a familiar concept with definitions for distances and angles stemming directly from the Euclidean norm, defined by the standard inner-product. In transitioning to generic differentiable manifolds, these familiar definitions no longer hold and a generalised mathematical framework is required. In this section we first introduce the concept of Riemannian manifolds, endowed with a metric to enable computation of the inner product on the tangent space. We then leverage this metric to provide a notion of directional derivatives and conditions required to transport a vector along the manifold in such a manner that parallelism is maintained. We take the idea of parallel transport and define geodesics, the generalisation of straight lines on the manifold. Finally, we comment on the computational framework employed throughout this paper, utilising automatic differentiation to compute quantities of interest. We refer the reader to Lee [5], do Carmo [6] for a more extensive overview of differential geometry where necessary.

### 2.1 Riemannian Manifolds

A Riemannian manifold [5] is a pair  $(M, g)$ , where  $M$  is a smooth manifold, and  $g$  is a choice of Riemannian metric on  $M$ . This metric allows us to compute a smooth  $(0, 2)$ -tensor field whose value  $g_p$  at a point  $p \in M$  is an inner product on the tangent space,  $T_p M$ . Components of the metric are defined as  $g_{ij}(p) = \langle \partial_i|_p, \partial_j|_p \rangle$ , where  $\partial_i = \partial/\partial x^i$  denotes the  $i$ th coordinate vector field. For arbitrary vectors  $v, w \in T_p M$ , we can compute the inner product

$$\langle v, w \rangle_g = \langle v^i \partial_i|_p, w^j \partial_j|_p \rangle = g_p(v, w) = g_{ij} v^i w^j, \quad (1)$$

providing the ability to compute distances and angles on the tangent-plane. Note that here, and throughout this paper, we use the Einstein summation convention in conjunction with notation  $x^i, x_i$  to denote contravariant and covariant vectors accordingly. To provide a connection to Euclidean space, we consider the Euclidean metric  $\tilde{g}_{ij} = \delta_{ij}$ ; this allows us to recover our standard definition of the inner product for Euclidean spaces,  $\langle v, w \rangle_{\tilde{g}} = v^i w^i$ . An important point of note is that every smooth manifold admits a Riemannian metric.

We next consider the case of embedded submanifolds. Suppose  $(\tilde{M}, \tilde{g})$  is a Riemannian manifold and  $M \subseteq \tilde{M}$  is an embedded submanifold. Given a smooth immersion  $\iota : M \hookrightarrow \tilde{M}$ , the metric  $g = \iota^* \tilde{g}$  is referred to as the metric induced by  $\iota$ , where  $\iota^*$  is the pullback. If  $(M, g)$  is a Riemannian submanifold of  $(\tilde{M}, \tilde{g})$ , then for every  $p \in M$  and  $v, w \in T_p M$ , the induced metric is defined as

$$g_p(v, w) = \tilde{g}_p(d\iota_p(v), d\iota_p(w)). \quad (2)$$

This statement forms the guiding principle that allows us to compute metrics induced by differentiable function transformations. We leverage this idea to define the metric induced by an autoencoder.

### 2.2 Covariant Differentiation & Parallel Transport

Given a definition for the inner product on the manifold, we can introduce the notion of covariant differentiation; a means of specifying derivatives along tangent vectors. For a vector  $w \in T_p M$  and a vector field  $v \in TM$ , we define the covariant derivative as

$$\nabla_v w = v^j \nabla_{\partial_j} w^i \partial_i = (v^j w^k_{;j}) \partial_k = (v^j w^k_{;j} + \Gamma^k_{ij} v^j w^i) \partial_k, \quad (3)$$

where; for brevity, we introduce the notation  $w^k_{;j}, w^k_{;j}$  to denote the partial, and covariant derivative respectively – each taken with respect to the  $j$ th coordinate vector field. The expression containing

the summation in Eq. 3 provides an intuitive explanation for the concept of covariant differentiation: the first term represents the standard directional derivative; and the second term is responsible for quantifying the ‘twisting’ of the coordinate system. The term  $\Gamma_{ij}^k$  is referred to as the Christoffel symbol of the second kind, or the affine connection; providing a measure of how the basis changes over the manifold. We define the Christoffel symbols as

$$\Gamma_{ij}^k = \partial_j(\partial_i) \cdot \partial^k = \frac{1}{2}g^{km} (g_{mi,j} + g_{mj,i} - g_{ij,m}), \quad (4)$$

where  $\partial^k = g^{km}\partial_m$  is the index-raised coordinate vector field, and  $g^{km}$  is the inverse of the metric tensor  $g_{km}$ . In the absence of covariant differentiation, transporting a vector  $w \in T_pM$  along the manifold does not guarantee it remains parallel to itself in the tangent planes along the path. Our definition of the covariant derivative provides a sufficient condition to ensure the parallelism is conserved along a trajectory. Mathematically we express this as

$$\nabla_v w = v^j w_{,j}^k + \Gamma_{ij}^k v^j w^i = 0. \quad (5)$$

The ability to preserve parallelism in the tangent plane along a trajectory on the manifold provides us with the ability to define curves of interest, namely geodesics.

### 2.3 Geodesics

A geodesic on the manifold generalises the notion of a straight line between points. This geodesic curve  $\gamma(\lambda)$  is locally length-minimising in the sense that it constitutes a solution of the Euler-Lagrange equations: it describes the motion of a rigid body devoid of acceleration. Leveraging our definition of covariant differentiation, we can describe a geodesic as a curve  $\gamma(\lambda)$  whose tangent vectors remain parallel to themselves as they are transported along the curve, yielding the geodesic equation

$$\nabla_{\dot{\gamma}} \dot{\gamma} = \ddot{\gamma}^k + \Gamma_{ij}^k \dot{\gamma}^i \dot{\gamma}^j = 0, \quad (6)$$

where derivatives  $\ddot{\gamma}, \dot{\gamma}$  are taken with respect to the affine parameter  $\lambda$ . This geodesic equation ensures the speed  $\langle \dot{\gamma}, \dot{\gamma} \rangle_g^{0.5}$  is constant along the trajectory, allowing us to classify parameterisations  $\lambda \in [0, 1]$  as unit-speed geodesics. Conversely, the geodesic can be parameterised with respect to length to yield a unit-distance geodesic.

A geodesic  $\gamma$  is said to be minimising *iff* there exist no shorter, valid geodesics with the same endpoints. The length of this minimising geodesic provides a notion of geodesic distance on the manifold. While we can validate that a curve is a geodesic, there is no principled way to demonstrate that the length-minimising curve has been obtained. In this work we address two key points: providing principled means to obtain valid geodesics on arbitrary manifolds, such as those induced by machine learning models; and computing geodesic distance fields directly.

### 2.4 Computational Framework

In this paper we provide a computational framework for operating on differentiable manifolds. We leverage the automatic differentiation capabilities of *jax* [16] to compute the metric induced by an arbitrary, smooth immersion as described in Eq. 2, as well as all derivative properties. We provide access to our open source library on Github.<sup>1</sup>

## 3 Computing Geodesics

Computing valid geodesics on differentiable manifolds has applications in many domains, not least computer vision [17], general relativity [18], and machine learning [19]. In this section we introduce a principled numerical approach to computing valid geodesics on differentiable manifolds. We first define the initial value problem and demonstrate a numerical scheme which ensures energy conservation along the resultant geodesic. Next, we address the important problem of obtaining geodesics connecting points on the manifold; this is presented as a boundary value problem for which

<sup>1</sup>All code is available on GitHub: [https://github.com/removed\\_for\\_anonymity](https://github.com/removed_for_anonymity)

we outline numerical schemes which allow us to obtain valid geodesics. We then outline and discuss an approach for obtaining length-minimising curves adopted by the machine learning community. Finally, we demonstrate the application of these methods on a manifold induced by an autoencoder, comparing the ability of these approaches to produce valid geodesics.

### 3.1 On the Straight and Narrow: Initial Value Problem

We first consider the initial value problem, defining unit-speed geodesics  $\gamma : [0, 1] \rightarrow M$ . Given a point  $p \in M$ , and an initial velocity vector  $v \in T_p M$ , we wish to compute the unique geodesic  $\gamma(\lambda)$  such that  $\gamma(0) = p, \dot{\gamma}(0) = v$ . We express the initial value problem through the exponential map

$$\gamma(\lambda = 1) = \exp_p(v) \quad (7)$$

The geodesic equation, as defined in Eq. 5, is a second-order ordinary differential equation expressed in Lagrangian coordinates. As the geodesic equation is a solution to the Euler-Lagrange equations, this admits the Hamiltonian

$$H(q, p) = \frac{1}{2} g^{ij} p_i p_j, \quad (8)$$

where  $g^{ij}$  is the inverse metric tensor, and  $p_i$  denotes the covariant conjugate momenta. This Hamiltonian formulation gives rise to an alternative definition of the geodesic equations

$$\dot{q}^i = \frac{\partial H}{\partial p_i} = g^{ij} p_j \quad \dot{p}_i = -\frac{\partial H}{\partial q^i} = -\frac{1}{2} g^{jk}_{,i} p_j p_k, \quad (9)$$

which ensures energy conservation along the geodesics, as demonstrated by

$$\frac{dH}{dt} = \frac{\partial H}{\partial q^k} \dot{q}^k + \frac{\partial H}{\partial p_k} \dot{p}_k = -\dot{p}_k \dot{q}^k + \dot{q}^k \dot{p}_k = 0. \quad (10)$$

In computing the exponential map  $\exp_p(v)$ , we wish to leverage an integration scheme which conserves the Hamiltonian along the resulting trajectory; a task best suited for symplectic integration. While classical integration schemes are often subject to energy dissipation, symplectic integration methods are designed in such a manner as to provide an error bound for the energy dissipation; an important characteristic for energy-conserving systems. Conventional symplectic integration schemes [20], such as the likes of symplectic Euler, velocity Verlet, rely on a separable Hamiltonian – a property not exhibited by the geodesic equation.

We employ a symplectic integration scheme for nonseparable Hamiltonians proposed by Tao [21]. The Hamiltonian is augmented in an extended phase space with symplectic 2-form  $dq \wedge dp + dx \wedge dy$

$$\bar{H}(q, p, x, y) := H_A + H_B + \omega H_C, \quad (11)$$

where  $H_A = H(q, y), H_B = H(x, p)$  represent copies of the original system with mixed positions and momenta;  $H_C = 1/2 \|q - x\|_2^2 + 1/2 \|p - y\|_2^2$  is an artificial restraint for the energy conservation; and  $\omega$  is a constant which determines the strength of the relationship between the two copies.

Strang-splitting [22, 23] is employed to generate a flow-map for a second-order integrator

$$\phi_2^\delta := \phi_{H_A}^{\delta/2} \circ \phi_{H_B}^{\delta/2} \circ \phi_{\omega H_C}^\delta \circ \phi_{H_B}^{\delta/2} \circ \phi_{H_A}^{\delta/2}, \quad (12)$$

where individual flow-map components constitute the integration step. This integration scheme can be extended to arbitrary higher-order schemes through use of the Yoshida triple-jump [24]

$$\phi_l^\delta := \phi_{l-2}^{\psi_l \delta} \circ \phi_{l-2}^{(1-2\psi_l)\delta} \circ \phi_{l-2}^{\psi_l \delta}, \quad \text{where } \psi_l = \frac{1}{2 - 2^{1/(l+1)}}, \quad (13)$$

and  $l$  is the desired order of integration. For the purposes of this work, we employ a fourth-order symplectic integration scheme,  $l = 4$ .

### 3.2 Connecting the Dots: Boundary Value Problem

Given points  $p, q \in M$ , we wish to find the geodesic  $\gamma : [0, 1] \rightarrow M$  which connects these points. Using our definition of the exponential map, we can express this as  $q = \exp_p(v)$ , where we wish to find the initial tangent vector  $v \in T_p M$ . This formulation results in a two-point boundary value problem for which standard shooting methods can be applied [25]. We define the residual

$$r(v) = \exp_p(v) - q = 0, \quad (14)$$

where the exponential map  $\exp_p(v)$  is computed using the symplectic integration scheme described in §3.1. Roots of the residual  $r(v)$  denote solutions to the boundary value problem, expressible using the logarithmic map  $v = \log_p(q)$ ; a natural inverse to the exponential map [6]. We employ the standard Newton-Raphson root-finding method to obtain solutions to the boundary value problem and find valid geodesics connecting two points. We note that this shooting method finds locally length-minimising geodesics, not necessarily the shortest geodesics.

### 3.3 Length-Minimising Geodesics

Geodesics are defined as locally shortest paths on the manifold – solutions to the Euler-Lagrange equations. In many circumstances there are multiple geodesics connecting two points, each with different lengths. We define the length of a geodesic as

$$L(\gamma) = \int_0^1 \langle \dot{\gamma}(t), \dot{\gamma}(t) \rangle_{\gamma(t)}^{1/2} dt. \quad (15)$$

The geodesic distance  $d_g(p, q)$  between two points  $p, q \in M$  is defined as infimum of the length of all valid geodesics which connect the two points; that is

$$d_g(p, q) = \inf_{\gamma} \{L(\gamma) : \gamma(0) = p, \gamma(1) = q\}. \quad (16)$$

Conversely, this admits that the shortest curve between two points is itself a valid geodesic. Work by Chen et al. [13] leverages the notion that the shortest curve connecting two points on the manifold yields a valid geodesic, admitting the geodesic distance  $d_g(p, q)$ . In their proposed methodology a neural network  $\gamma_{\theta} : [0, 1] \rightarrow M$ , constrained with the boundary values  $\gamma_{\theta}(0) = p, \gamma_{\theta}(1) = q$ , parameterises the target geodesic. Parameters  $\theta$  are optimised in accordance with the objective of minimising the length of the resultant curve, as per Eq. 15. This proposed approach has been adopted by the machine learning community to compute distances and produce geodesic paths on latent manifolds [26, 27].

Obtaining valid geodesics, and thus the geodesic distance, is reliant on the solution to a global optimisation problem. In the event that the resultant curve is not a geodesic, there must exist a valid geodesic with shorter length. That is to say

$$d_g(p, q) < L(\gamma_{\theta}) \quad \text{when} \quad \theta \neq \theta^*, \quad (17)$$

where  $\theta^*$  denotes the globally optimum parameters. There is also no guarantee that the network architecture used to parameterise  $\gamma_{\theta}$  even has the capacity to represent the true geodesic. Although the approach is well-justified, we find that the model is prone to getting stuck in local minima and that converged solutions do not produce valid geodesics. We examine the ability of this approach to produce valid geodesics in §3.4 and compare results to the principled numerical integration approach.

### 3.4 Interpolation on an Autoencoder manifold.

We compare the aforementioned approaches by computing paths on a manifold defined by an autoencoder  $\eta_{\theta} = \eta_{\theta}^e \circ \eta_{\theta}^d$ , where  $\eta_{\theta}^e : \mathbb{R}^n \rightarrow M$  represents the encoder, and  $\eta_{\theta}^d : M \rightarrow \mathbb{R}^n$  the decoder. An autoencoder with latent dimensionality  $z \in M \subset \mathbb{R}^2$  is pre-trained on the MNIST dataset [28], with the resulting latent space representing intrinsic coordinates on the manifold. Using our definition of the induced metric per Eq. 2, we define the metric induced by the decoder [4, 13] as

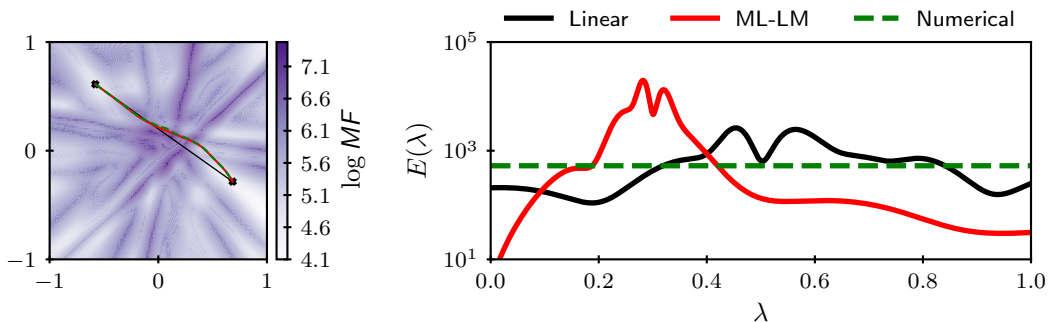
$$g_{ij}(z) = \frac{\partial \eta_{\theta}^d(z^k)}{\partial z^i} \frac{\partial \eta_{\theta}^d(z^k)}{\partial z^j}. \quad (18)$$

In order to provide a visualisation of the manifold, we compute the magnification factor,  $MF$ , across the domain. The magnification factor denotes the rate of change of infinitesimal volume, mapping a point on the manifold to Euclidean space; precisely  $MF = \sqrt{\det g_{ij}}$ .

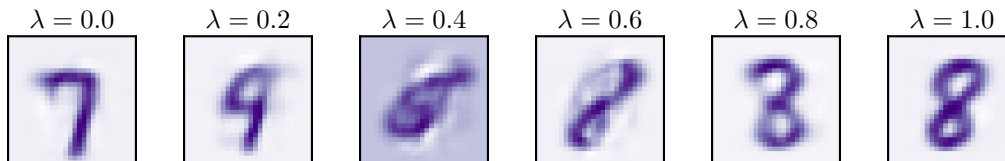
We consider trajectories  $\gamma(\lambda)$  between points  $z_1, z_2 \in M$  on the resulting manifold. Results in Figure 1a demonstrate three independent trajectories between these points on the manifold, corresponding to: linear interpolation; the length-minimising (ML-LM) curve as described in §3.3; and a valid geodesic produced by integration of the geodesic equation, as described in §3.2. In each case, we obtain a curve  $\gamma : [0, 1] \rightarrow M$ . A time-step of  $\Delta t = 10^{-3}$  is employed, yielding a trajectory with 1000 time-steps. The network parameterising the length-minimising curve is obtained using an ensemble of 30 networks, each trained with the *adam* optimiser [29]. For the numerical integration, a fourth-order symplectic integration scheme is used with  $\omega = 10^{-2}$ . Further details of network architecture and training details can be found in the supplementary material.

Trajectories for the length-minimising curve and the valid geodesic are noticeably similar with regard to the resulting coordinates, however the energy along each trajectory provides more insight. We observe that the trajectories produced by linear interpolation and the length-minimising curve approach are subject to large degrees of energetic deviation, violating the Hamiltonian-preserving properties of the geodesic equation. These energy fluctuations present in the ML-LM approach invalidate the ability to compute distance in a meaningful way, a fundamental flaw of the existing approach. The trajectory obtained from numerical integration yields a valid geodesic, exhibiting energy conservation along the path; this makes it much more effective for latent interpolation as well as distance computation.

Samples can be drawn along the resulting trajectory to provide a form of latent interpolation. Realisations shown in Figure 1b depict samples drawn along the valid numerical trajectory, drawing samples  $\eta_{\theta}(\gamma(\lambda))$ ,  $\lambda \in \{0.0, 0.2, 0.4, 0.6, 0.8, 1.0\}$ . Interpolation along an energy-conserving curve yields a smoother transition when compared with the alternative approaches. This has numerous applications for latent space interpolation, such as that used in generative modeling.



(a) Latent trajectories  $\gamma(\lambda)$  for the three interpolation schemes are shown against a background of magnification factor,  $MF$  on the left; and energy,  $E = \langle \dot{\gamma}, \dot{\gamma} \rangle_g$  along each trajectory is shown on the right. We observe constant energy for the numerical trajectory, a result of solving the geodesic equation directly on the manifold.



(b) Decoder realisations  $\eta_{\theta}^d(\gamma(\lambda))$  of samples drawn from numerical geodesic trajectory. By conserving energy along the interpolation trajectory we are able to obtain smooth transitions between points on the manifold.

Figure 1: Interpolation on the manifold induced by an autoencoder trained on the MNIST dataset.

## 4 Distance Fields: Solutions to the Eikonal Equation

Obtaining length-minimising geodesics between pairwise points is challenging, as discussed in §3; instead, we introduce an alternative approach to computing geodesic distances. Given a point  $p \in M$ , we consider a function  $\phi : p \mapsto d_g(p, q)$  which computes the geodesic distance to an arbitrary point  $q \in M$ . The resultant distance function is a solution to the Eikonal equation

$$\|\nabla\phi\| = 1 \quad \text{s.t.} \quad \phi|_p = 0. \quad (19)$$

We generalise the notion of the Eikonal equation to the manifold, leveraging our definition of the inner product and using the exterior derivative. Upon manipulation, this yields

$$\langle \text{grad } \phi, \text{grad } \phi \rangle_g = g_{ij} \phi^{;i} \phi^{;j} = 1, \quad (20)$$

where  $\phi^{;i} = g^{ij} \phi_{;j}$  denotes the index-raised covariant derivative. For a distance function  $\phi$ , the gradient of the distance field provides the geodesic flow,  $\nabla\phi$ . This flow satisfies the geodesic equation

$$\nabla_{\nabla\phi} \nabla\phi = 0, \quad (21)$$

where integral paths constitute unit-distance geodesics travelling orthogonal to the level-sets imposed by the distance field. As a by-product of computing the distance function  $\phi$ , we are able to compute the length-minimising geodesics. We refer the reader to Lee [see 5, Thm. 6.31, 6.32] for a more rigorous overview on geodesic flows, and solutions to the Eikonal equation on the manifold.

While solutions to the Eikonal equation on the manifold have been considered previously, these methods leverage a series of approximations and discretisations to obtain solutions. Most notable are heat kernel methods which rely on numerical approximations to the Laplace-Beltrami operator, the dirac-delta distribution, and Varadhan's formula [12, 30, 31]. We propose an approach for working with continuous function representations, relying on no such approximations.

We parameterise the distance field by a neural network  $\phi_\theta : M \rightarrow \mathbb{R}_{\geq 0}$ , architecturally constrained in such a manner as to ensure  $\phi_\theta(p) = 0$ . The solution is posed as an optimisation problem

$$\theta^* = \arg \min_{\theta} \mathcal{L}(\epsilon_\phi, \epsilon_{\nabla\phi}) \quad \text{where} \quad \epsilon_\phi = g_{ij} \phi_\theta^{;i} \phi_\theta^{;j} - 1, \quad \epsilon_{\nabla\phi} = \langle \nabla_{\nabla\phi_\theta} \nabla\phi_\theta, \nabla_{\nabla\phi_\theta} \nabla\phi_\theta \rangle_q \quad (22)$$

Naturally, the solution to the Eikonal equation is more sensitive in regions of high curvature; a consequence of induced geodesic deviation. We introduce a novel sampling and loss-scaling methodology to ensure we are able to capture the solution appropriately in regions of high curvature.

### 4.1 Introducing the Curvature

The Riemann curvature tensor  $R_{ijk}^l$  provides a means to represent the curvature on the manifold. Mathematically, this curvature denotes the failure of the second covariant derivatives to commute, constituting the tidal force experienced by a rigid body moving along a geodesic. A Riemannian manifold has zero curvature in regions exhibiting local isometry to Euclidean space. In the interest of obtaining a scalar value for the curvature, we introduce the following progression

$$R_{ijk}^l = \Gamma_{ik,j}^l - \Gamma_{ij,k}^l + \Gamma_{jm}^l \Gamma_{ik}^m - \Gamma_{km}^l \Gamma_{ij}^m \quad \rightarrow \quad R_{ij} = R_{imj}^m \quad \rightarrow \quad R = g^{ij} R_{ij} \quad (23)$$

where  $R_{ijk}^l$  denotes the Riemann curvature tensor;  $R_{ij}$  the Ricci curvature tensor, obtained by contracting over the first and third indices; and  $R$  is the Ricci scalar, the trace of the Ricci tensor with respect to the metric. The Ricci scalar is a local invariant on the manifold and assigns a single real number to the curvature at a particular point. We note that the demonstrated progression relies solely on the definition of the metric tensor  $g_{ij}$ .

As a result of geodesic deviation exhibited in regions of high curvature, the geodesic flow  $\nabla\phi$ , and consequently the distance field  $\phi_\theta$ , are more challenging to characterise. We leverage information about the curvature to provide a training mechanism which takes this into account.

## 4.2 Leveraging the Curvature

We propose a novel sampling and scaling strategy for the loss, utilising information about the local scalar curvature of the manifold. Employing the Metropolis-Hastings [32, 33] sampling algorithm, we draw samples in regions of the manifold which exhibit high-degrees of local scalar curvature. To ensure a representative distribution, we sample multiple chains and discard initial samples to ensure convergence of the Markov chain. A kernel density estimate is obtained for the resulting points to obtain a probability density function to allow efficient sampling in the training process.

We propose a loss function which scales the residuals based on the degree of local curvature

$$\mathcal{L} = \frac{1}{|\mathcal{X}|} \sum_{x \in \mathcal{X}} \psi(x) [\epsilon_\phi(x)^2 + \lambda \epsilon_{\nabla\phi}(x)] \quad \text{where} \quad \psi(x; \alpha) = 1 + \alpha \log(1 + R(x)), \quad (24)$$

where  $x \in \mathcal{X}$  are training samples;  $\lambda$  is a weighting term for the residual losses; and  $\alpha$  is a scaling factor used to determine the relative importance of the local curvature. For the sake of this work, we take  $\lambda = 10^{-3}$ ,  $\alpha = 10^{-1}$ , empirically determined to provide satisfactory convergence. Training samples  $\mathcal{X}$  are drawn from a distribution  $\mathcal{D}$  which is the average of a uniform distribution over the domain, and the probability density function generated from the curvature samples. This proposed loss function is used as the objective function in the optimisation problem posed in Eq. 22.

In order to provide an interpretable example, we demonstrate results for a function  $f : \mathbb{R}^2 \rightarrow \mathbb{R}^3$ , where intrinsic coordinates are interpretable in a two-dimensional space. We choose a complex manifold with a multitude of local extrema, based on the *peaks* function [34], namely

$$f : (x, y) \mapsto 3(1 - x)^2 e^{-x^2 - (y+1)^2} - 10 \left( \frac{x}{5} - x^3 - y^5 \right) e^{-x^2 - y^2} - \frac{1}{3} e^{-(x+1)^2 - y^2}. \quad (25)$$

A demonstration of the manifold, as well as the loss scaling and sampling strategy can be seen in Figure 2a. We observe that regions of high scalar curvature are subjected to higher degrees of penalisation in the loss term, and additional samples for training are drawn from the curvature distribution. This combination of scaling and sampling is effective in overcoming challenges to obtaining a solution to the Eikonal equation.

Results in Figure 2b demonstrate the predicted geodesic distance on the manifold from a point  $p$ . We observe that the distance field conforms to the manifold, as represented by the level-set contours; this is a consequence of re-formulating the Eikonal equation to account for the imposed metric tensor. The level-sets of the resultant distance field are shown in Figure 21, with arrows showing the geodesic flow  $\nabla\phi_\theta$  on the manifold. As expected, the geodesics flow orthogonal to the level sets imposed by the distance field  $\phi_\theta$  and provide geodesic paths.

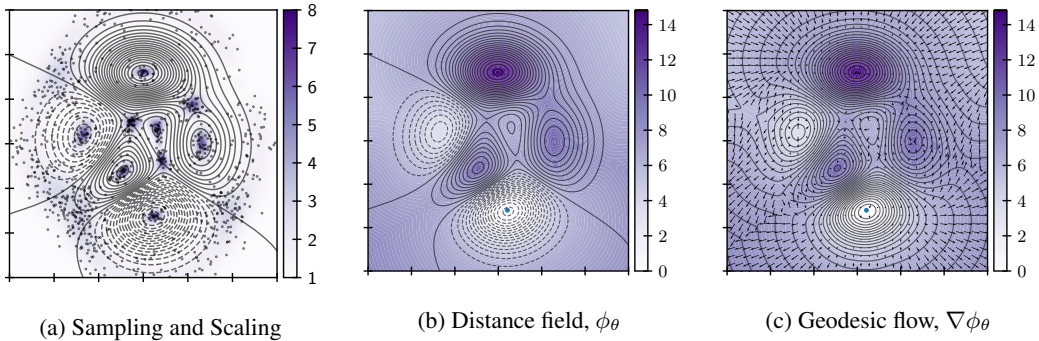


Figure 2: Solutions to the Eikonal equation: (a) demonstrates the curvature scaling field,  $\psi(x; \alpha = 1)$ , and corresponding samples drawn from the scalar curvature distribution; (b) shows the geodesic distance predicted by the network,  $\phi_\theta$ ; and (c) shows the resulting geodesic flow,  $\nabla\phi_\theta$ .



## 5 Conclusions

In this work we first introduce a numerical methodology for computing geodesics on differentiable manifolds. An autoencoder is pre-trained on the MNIST dataset, inducing a Riemannian metric which allows us to operate in a principled manner on the resulting latent space. We consider the task of interpolation in the latent space and compare trajectories obtained by: linear interpolation; a machine learning approach for obtaining length-minimising curves; and our numerical method. Conservation of energy along the latent trajectory is a core principle for valid geodesics. We demonstrate that only the numerical approach was able to achieve valid geodesics, satisfying the geodesic equation, and demonstrating energy conservation. The ability to produce valid geodesics allows for smooth interpolation, imperative for applications in generative modelling, and reduced-order modelling.

We then address the problem of computing geodesic distance, providing a means to obtain a model-based parameterisation of distance fields and geodesic flows on differentiable manifolds. Our proposed methodology relies on a manifold-informed extension to the Eikonal equation, allowing us to obtain a continuous function representation, without unnecessary assumptions or approximations. Key to this is a novel sampling and scaling training mechanism which leverages information about the curvature of the manifold to stabilise training in regions subject to significant geodesic deviation. We demonstrate the ability to produce distance fields which conform to the manifold, a consequence of imposing knowledge of the metric throughout the training process.

## Acknowledgments and Disclosure of Funding

D. Kelshaw. and L. Magri. acknowledge support from the UK EPSRC and thank Marika Taylor for fruitful discussions. L. Magri gratefully acknowledges financial support from the ERC Starting Grant PhyCo 949388.

## References

- [1] C. Fefferman, S. Mitter, and H. Narayanan, “Testing the manifold hypothesis,” *Journal of the American Mathematical Society*, vol. 29, no. 4, pp. 983–1049, Oct. 2016.
- [2] G. E. Hinton and R. R. Salakhutdinov, “Reducing the Dimensionality of Data with Neural Networks,” *Science*, vol. 313, no. 5786, pp. 504–507, Jul. 2006.
- [3] G. E. Hinton and R. Zemel, “Autoencoders, Minimum Description Length and Helmholtz Free Energy,” in *Advances in Neural Information Processing Systems*, vol. 6. Morgan-Kaufmann, 1993.
- [4] L. Magri and A. K. Doan, “On interpretability and proper latent decomposition of autoencoders,” Dec. 2022.
- [5] J. M. Lee, *Introduction to Riemannian Manifolds*, ser. Graduate Texts in Mathematics. Cham: Springer International Publishing, 2018, vol. 176.
- [6] M. P. do Carmo, *Differential Geometry of Curves & Surfaces*, revised & updated second edition ed. Mineola, New York: Dover Publications, INC, 2018.
- [7] G. Arvanitidis, L. K. Hansen, and S. Hauberg, “Latent Space Oddity: On the Curvature of Deep Generative Models,” Dec. 2021.
- [8] P. Bojanowski, A. Joulin, D. Lopez-Paz, and A. Szlam, “Optimizing the Latent Space of Generative Networks,” May 2019.
- [9] J. Page, M. P. Brenner, and R. R. Kerswell, “Revealing the state space of turbulence using machine learning,” *Physical Review Fluids*, vol. 6, no. 3, p. 034402, Mar. 2021.
- [10] A. Racca, N. A. K. Doan, and L. Magri, “Modelling spatiotemporal turbulent dynamics with the convolutional autoencoder echo state network,” Nov. 2022.

- [11] H. Kim, H. Park, and H. Zha, “Distance Preserving Dimension Reduction for Manifold Learning,” in *Proceedings of the 2007 SIAM International Conference on Data Mining*. Society for Industrial and Applied Mathematics, Apr. 2007, pp. 527–532.
- [12] K. Crane, C. Weischedel, and M. Wardetzky, “Geodesics in heat: A new approach to computing distance based on heat flow,” *ACM Transactions on Graphics*, vol. 32, no. 5, pp. 1–11, Sep. 2013.
- [13] N. Chen, A. Klushyn, R. Kurle, X. Jiang, J. Bayer, and P. van der Smagt, “Metrics for Deep Generative Models,” Feb. 2018.
- [14] M. Bačák, “Computing Medians and Means in Hadamard Spaces,” *SIAM Journal on Optimization*, vol. 24, no. 3, pp. 1542–1566, Jan. 2014.
- [15] X. Pennec, “Intrinsic Statistics on Riemannian Manifolds: Basic Tools for Geometric Measurements,” *Journal of Mathematical Imaging and Vision*, vol. 25, no. 1, pp. 127–154, Jul. 2006.
- [16] J. Bradbury, R. Frostig, P. Hawkins, M. J. Johnson, C. Leary, D. Maclaurin, G. Necula, A. Paszke, J. VanderPlas, S. Wanderman-Milne, and Q. Zhang, “JAX: Composable transformations of Python+NumPy programs,” 2018.
- [17] G. Peyré, “Geodesic Methods in Computer Vision and Graphics,” *Foundations and Trends® in Computer Graphics and Vision*, vol. 5, no. 3-4, pp. 197–397, 2009.
- [18] S. M. Carroll, *Spacetime and Geometry: An Introduction to General Relativity*. San Francisco: Addison Wesley, 2004.
- [19] M. M. Bronstein, J. Bruna, T. Cohen, and P. Veličković, “Geometric Deep Learning: Grids, Groups, Graphs, Geodesics, and Gauges,” May 2021.
- [20] *Geometric Numerical Integration*, ser. Springer Series in Computational Mathematics. Berlin/Heidelberg: Springer-Verlag, 2006, vol. 31.
- [21] M. Tao, “Explicit symplectic approximation of nonseparable Hamiltonians: Algorithm and long time performance,” *Physical Review E*, vol. 94, no. 4, p. 043303, Oct. 2016.
- [22] G. Strang, “On the Construction and Comparison of Difference Schemes,” *SIAM Journal on Numerical Analysis*, vol. 5, no. 3, pp. 506–517, Sep. 1968.
- [23] R. I. McLachlan and G. R. W. Quispel, “Splitting methods,” *Acta Numerica*, vol. 11, pp. 341–434, Jan. 2002.
- [24] H. Yoshida, “Construction of higher order symplectic integrators,” *Physics Letters A*, vol. 150, no. 5-7, pp. 262–268, Nov. 1990.
- [25] H. B. Keller, *Numerical Solution of Two Point Boundary Value Problems*. Society for Industrial and Applied Mathematics, Jan. 1976.
- [26] G. Tennenholtz and S. Mannor, “Uncertainty Estimation Using Riemannian Model Dynamics for Offline Reinforcement Learning,” in *Advances in Neural Information Processing Systems*, Oct. 2022.
- [27] G. Arvanitidis, S. Hauberg, and B. Schölkopf, “Geometrically Enriched Latent Spaces,” Aug. 2020.
- [28] L. Deng, “The mnist database of handwritten digit images for machine learning research,” *IEEE Signal Processing Magazine*, vol. 29, no. 6, pp. 141–142, 2012.
- [29] D. P. Kingma and J. Ba, “Adam: A Method for Stochastic Optimization,” Jan. 2017.
- [30] S. R. S. Varadhan, “On the behavior of the fundamental solution of the heat equation with variable coefficients,” *Communications on Pure and Applied Mathematics*, vol. 20, no. 2, pp. 431–455, 1967.

- [31] A. Gropp, L. Yariv, N. Haim, M. Atzmon, and Y. Lipman, “Implicit Geometric Regularization for Learning Shapes,” Jul. 2020.
- [32] N. Metropolis, A. W. Rosenbluth, M. N. Rosenbluth, A. H. Teller, and E. Teller, “Equation of state calculations by fast computing machines,” *The journal of chemical physics*, vol. 21, no. 6, pp. 1087–1092, 1953.
- [33] W. K. Hastings, “Monte Carlo sampling methods using Markov chains and their applications,” 1970.
- [34] “Peaks function - MATLAB peaks,” <https://www.mathworks.com/help/matlab/ref/peaks.html>.

## Supplementary Material

### Training Details: Latent Interpolation

For the task of latent interpolation, we train a standard autoencoder on the MNIST dataset. The network  $\eta_\theta$ , tasked with learning the identity function  $\eta_\theta : x \mapsto x$ , consists of an encoder  $\eta_\theta^e$  and decoder  $\eta_\theta^d$ . A precise definition is given by

$$\eta_\theta = \eta_\theta^e \circ \eta_\theta^d, \quad \text{where} \quad \eta_\theta^e = \sigma(\eta_\theta^{e1}) \circ \sigma(\eta_\theta^{e2}), \quad \eta_\theta^d = \sigma(\eta_\theta^{d1}) \circ \eta_\theta^{d2}$$

$$\begin{array}{ll} \eta_\theta^{e1} : \mathbb{R}^{784} \rightarrow \mathbb{R}^{32} & \eta_\theta^{d1} : \mathbb{R}^2 \rightarrow \mathbb{R}^{32} \\ \eta_\theta^{e2} : \mathbb{R}^{32} \rightarrow \mathbb{R}^2 & \eta_\theta^{d2} : \mathbb{R}^{32} \rightarrow \mathbb{R}^{784} \end{array}$$

All intermediate layers  $\eta_\theta^{(\cdot)}$  are linear transformations, using activations  $\sigma : x \mapsto \tanh(x)$  to induce nonlinearities. The *adam* optimiser is used for training, employing a learning rate of  $3 \times 10^{-4}$ .

Data  $x \in \mathcal{X}$  is standardised to the range  $x \in [0, 1]$  before being fed to the network. We employ the standard data split using 50000 samples for training and 10000 for validation. Optimal parameters  $\theta^*$  are chosen to be those which minimise the reconstruction error on the validation set.

### Training Details: Eikonal Equation

The distance function is parameterised by a neural network  $\phi_\theta : M \rightarrow \mathbb{R}_{\geq 0}$  constrained to provide strictly positive outputs with  $d_g(q, q) = 0$ . This is achieved by transforming the outputs of a network

$$\phi_\theta : (p, q) \mapsto \left| \tilde{\phi}_\theta(p) - \tilde{\phi}_\theta(q) \right|,$$

where the unconstrained network  $\tilde{\phi}_\theta$  is defined by a sequence of transformations

$$\tilde{\phi}_\theta = \sigma \left( \tilde{\phi}_\theta^{(1)} \right) \circ \sigma \left( \tilde{\phi}_\theta^{(2)} \right) \circ \sigma \left( \tilde{\phi}_\theta^{(3)} \right) \circ \tilde{\phi}_\theta^{(4)}.$$

$$\begin{array}{ll} \tilde{\phi}_\theta^{(1)} : M \rightarrow \mathbb{R}^{64} & \tilde{\phi}_\theta^{(3)} : \mathbb{R}^{64} \rightarrow \mathbb{R}^{64} \\ \tilde{\phi}_\theta^{(2)} : \mathbb{R}^{64} \rightarrow \mathbb{R}^{64} & \tilde{\phi}_\theta^{(4)} : \mathbb{R}^{64} \rightarrow \mathbb{R}^1 \end{array}$$

Each transformation  $\tilde{\phi}_\theta^{(\cdot)}$  is a linear layer, and we choose an activation  $\sigma : x \mapsto \tanh(x)$  to induce nonlinearities. We consider the domain  $p \in [-3, 3] \subset \mathbb{R}^2$  and standardise inputs to the network to the range  $[-1, 1]$ . Training is conducted using a set of random samples drawn from the domain. A total of 20000 samples are drawn from the domain at each epoch: half drawn from a uniform distribution; the remaining half drawn from the distribution defined by the curvature. We employ the *adam* optimiser with a learning rate of  $3 \times 10^{-4}$  and train until we observe convergence.